Relative Intensity Noise and Four Wave Mixing in few mode VCSELs for PAM4 high speed modulation

Relative Intensity Noise and Four Wave Mixing in few mode VCSELs for PAM4 high speed modulation.

C. Rimoldi[1], M. Novarese[1], L: Minelli[1], L. L. Columbo[1], A. Tibaldi[1,2], S. Romero García[3], C. Raabe[3], R. Gaudino[1], P. Debernardi[2] and M. Gioannini[1]

1. Dipartimento di Elettronica e Telecomunicazioni, Politecnico di Torino, Corso Duca degli Abruzzi 24, IT-10129, Torino, Italy
2. Consiglio Nazionale delle Ricerca (CNR-IEIIT), Corso Duca degli Abruzzi 24, IT-10129, Torino, Italy
2. Cisco Optical, Nordostpark 12, D-90411, Nuremberg, Germany
mariangela.gioannini@polito.it

***Abstract*—We present a model, validated with experiments, to simulate few-modes VCSELs for high speed datacom. The model explains for the first time non-trivial characteristics observed in measured RIN spectra and high-resolution optical spectra as consequence of four wave mixing occurring in the laser active region.**

Keywords—VCSELs, high-speed datacom, relative intensity noise, multimode dynamics, TDECQ.

I. INTRODUCTION

Short-reach data transmission often employs few-mode VCSELs at 850nm and MMF for their low cost, low threshold current and high power, as required in intra-data center high speed energy efficient communications Standard circular aperture multi-mode VCSEL has typically quasi-degenerate higher order transverse modes, with emission wavelengths separated by a few GHz. While these modes are orthogonal to each other, their beatings give undesired peaks in the relative intensity noise (RIN) spectrum with an increase of the RIN integrated over the receiver bandwidth. A design of particular interest relies on VCSELs with elliptical oxide aperture [1]. By breaking the quasi-degeneracy of the transverse modes, a careful choice of the ellipticity arranges the mode frequency separations for beating tones outside the receiver bandwidth. We present an original coherent multi-mode VCSEL model that explains for the first time the origin of these unwanted beating tones. We validate our theoretical predictions against experimental results acquired for two different few-modes elliptical oxide aperture VCSELs with similar output power, both employed for high-speed data transmission. We then show how the model can be applied to interpret the non-trivial features in the optical and RIN spectra and to simulate transmitter characteristics such as eye diagram and TDECQ parameter for PAM 4 direct modulation at 53.125Gbaud.

II. MODEL AND EXPERIMENTS

In Fig. 1 we summarize the experimental results obtained for two elliptical oxide aperture few mode VCSELs (namely VCSEL A and VCSEL B). The two VCSELs are quite similar in terms of CW and modulation performance: threshold current of about 0.5mA, fiber coupled output power of more than 5mW and maximum intrinsic modulation bandwidth of 32 GHz. However, the measured RIN spectrum of VCSEL A displays various spurious peaks within the bandwidth of 40 GHz of our measurement set-up (Fig.1c). These peaks do not correspond to any frequency separation of the transverse modes of VCSEL A, since the two closest ones are C2 and C3 separated of about 90 GHz (Fig.1a). On the contrary, in Fig.1d we do not find spurious RIN peaks for VCSEL B in the 40 GHz bandwidth. Tiny sidebands (Fig.1a,b) are visible in the high-resolution optical spectra of both VCSELs. To understand these measurements, we have developed an original model to simulate the coherent interaction of the transverse modes in the quantum well active region and then predict the RIN characteristics and the side bands in the optical spectrum. Our model starts from the equation of the spatial and time evolution of the total electric field $E(\rho,\phi,t)$ and carrier density $N(\rho,\phi,t)$ in polar coordinates in the active region of the VCSEL. These are:

$$\frac{dE(\rho,\phi,t)}{dt} = -\frac{(1+i\alpha)}{2\tau_p}E(\rho,\phi,t) + \frac{\Gamma G_N(1+i\alpha)}{2}[N(\rho,\phi,t) - N_0]\frac{|E(\rho,\phi,t)|^2}{1+\varepsilon|E(\rho,\phi,t)|^2} + S_{sp}(\rho,\phi,t) \quad (1)$$

$$\frac{dN(\rho,\phi,t)}{dt} = \frac{\eta_i I(\rho,\phi,t)}{eV} - \frac{N(\rho,\phi,t)}{\tau_e} - \frac{n_g^2\epsilon_0 G_N}{2\hbar\omega_0}\frac{|E(\rho,\phi,t)|^2}{1+\varepsilon|E(\rho,\phi,t)|^2}[N(\rho,\phi,t) - N_0] + D\nabla_\perp^2 N(\rho,\phi,t), \quad (2)$$

where $I(\rho,\phi,t)$ is the current distribution in the active region as determined by the oxide aperture, τ_p is the photon lifetime, α the linewidth enhancement, G_N the differential gain, ε the gain compression factor, D the carrier diffusion coefficient, τ_e the carrier lifetime and S_{sp} a noise term accounting for spontaneous emission noise. The set of equations is numerically solved by expanding the total electric field as weighted sum of the transverse modes: $E(\rho,\phi,t) = \sum_m C_m(\rho,\phi)\tilde{E}_m(t)e^{-i\omega_m t}$ where ω_m is the lasing frequency and $C_m(\rho,\phi)$ is the transverse electric field profile of the lasing *m*-th mode. The mode profiles are approximated here with Hermite-Gauss modes (Fig.1e) but can be extracted e.g from experiments or electromagnetic simulations. Similarly, the carrier distribution is expanded in a basis of orthonormal functions; we choose a basis of Gauss-Laguerre modes B_k: $N(\rho,\phi,t) = \sum_m B_k(\rho,\phi)\widetilde{N_k}(t)$. With these expansions, we solve numerically a set of coupled differential equations in time and derive the time dynamics of the complex electric fields $\tilde{E}_m(t)$ of each mode and of the carrier density. Differently from other well-known VCSEL models implemented also in commercial simulators, we include here the coherent coupling between the electric field of the modes, the carrier density distribution (ie: spatial hole-

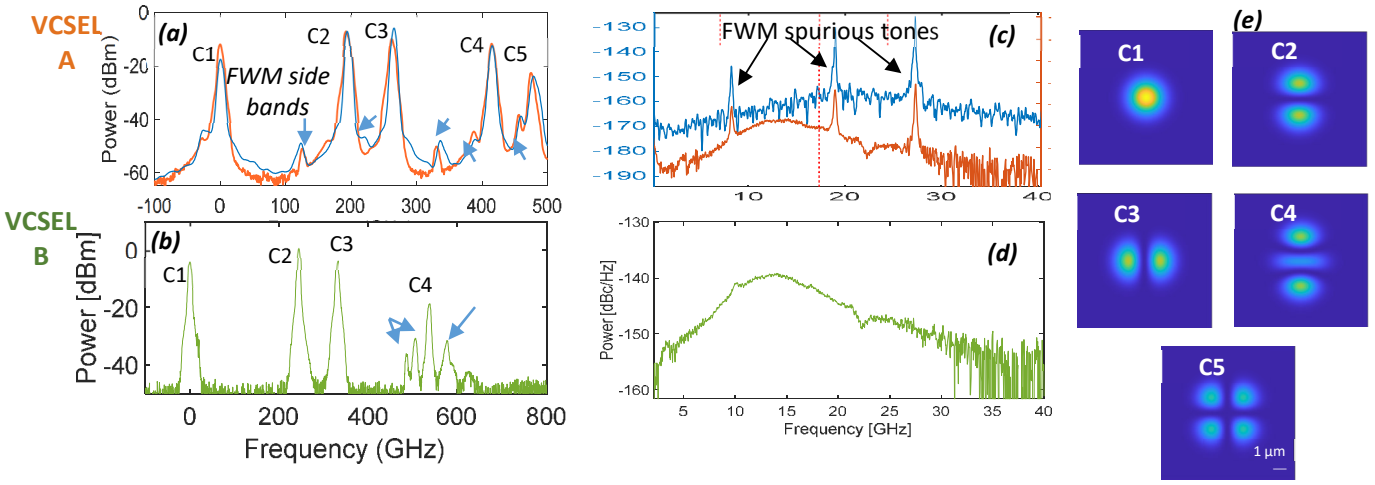

Fig. 1- Optical spectra (a,b) and spectral RIN (c,d) of VCSEL A at 4.5 mA and B at 3.5 mA; thin blue lines are the simulated optical spectra of VCSEL A. Modal field profiles of transverse modes $C_{1\text{-}5}$ considered in this work (e). Zero frequency in (a) and (b) corresponds to the wavelength of 850 nm; thick blue arrows evidence FWM side-bands in optical spectra.

burning) and its pulsations mediated by the mode beatings (ie: four wave mixing).

These are the essential and crucial ingredients to reproduce the RIN and the optical spectra in Fig. 1. To the best of our knowledge, there is no other model reported in the literature capable of explaining the spurious RIN peaks and the FWM side bands observed.

In more detail, under some realistic approximations, Eq. (1) can be reduced to:

$$\frac{d\tilde{E}_m}{dt} = -\frac{1+i\alpha}{2\tau_{p,m}}\tilde{E}_m + \tilde{g}\Lambda\tilde{E}_m - \gamma_{mmmm}\frac{|\tilde{E}_m|^2}{E_s^2}\tilde{E}_m - 2\sum_{n\neq m}\gamma_{mmnn}\frac{|\tilde{E}_n|^2}{E_s^2}\tilde{E}_m - \tilde{g}\Lambda\tilde{E}_m\sum_{n,l,r*}\gamma_{mnlr}\frac{\tilde{E}_n\tilde{E}_l\tilde{E}_r^*}{E_s^2}e^{i(\omega_{nm}+\omega_{lr})t} \quad (3)$$

with $\tilde{g} = \frac{\Gamma G_N(1+i\alpha)}{2}$, $E_s^2 = \frac{2\hbar\omega_0}{n_g^2\epsilon_0 G_N\tau_e}$, $\Lambda = \tau_e\left(\frac{\eta_i I}{eV} - \frac{N_0}{\tau_e}\right)$, and, $\gamma_{mnlr} = \int_0^\infty\int_0^{2\pi}\rho d\rho d\varphi\ \ C_m^* C_n C_l C_r^*$

In Eq. (3) the first term on the RHS accounts for cavity loss and the contribution of the α-parameter, the second term is stimulated emission, the third and fourth terms are the self-saturation and the cross-saturation induced on the m-th mode by the lasing of the n-th mode. The fifth term is the FWM mediated by carrier beating process causing tones of $\tilde{E}_m(t)$ at frequency $\omega_{nm} + \omega_{lr} = \omega_n - \omega_m + \omega_l - \omega_r$. When these beating tones fall within the RIN measurement bandwidth of our set-up, they are observable in the RIN spectrum as spurious peaks. For example, the spurious RIN peaks in Fig.1c are around $\nu_{45} + \nu_{32} = 7GHz$; $\nu_{53} + \nu_{12} = 18\ GHz$ and $\nu_{42} + \nu_{12} = 25\ GHz$. with ν_m the lasing frequency of mode C_m as measured from the optical spectra in Fig. 1a. For VCSEL B such tones remain outside the 40 GHz bandwidth but can yet be observed as side-bands of the optical spectrum. For example, peaks marked by arrows in Fig.1b are: sideband of C4 at 488 GHz due to beat-tone $\nu_{42} + \nu_{12} = 50\ GHz$ and sideband of C3 at 507 GHz due to $\nu_{32} + \nu_{32} = 173\ GHz$. Employing a set-up that scans the near-field of the VCSEL with a lensed fiber tip and by measuring the optical spectrum of the field collected, we reconstruct near-field patterns of the main modes and of side-bands. For example, the near-field of the side-band at 135 GHz in Fig. 1a is shown in Fig.2a together with the patterns of C2 at 232 GHz and C3 at 329 GHz. Fig. 2a clearly shows a pattern very similar to the spatial profile of C3 proving that this sideband is a tone of C3 with frequency $\nu_{23} + \nu_{23} = 194\ GHz$.

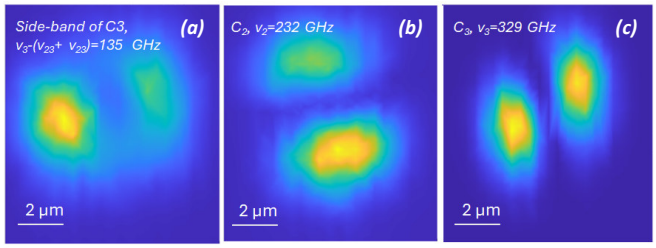

Fig.2 Measured field pattern of some frequencies of the optical spectrum in Fig. 1: sideband at 135 GHz, (b) mode C2 at 232 GHz and (c) C3 at 329 GHz.

To demonstrate the potential of our simulator, we simulate PAM4 modulation at 53.125 GBaud of VCSEL B. The back-to-back eye-diagram and eye after MMF propagation and equalization are in Fig. 3. The corresponding TDECQ parameter is 4.6 dB in qualitative agreement with experiments.

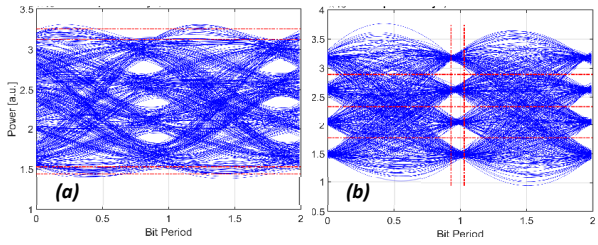

Fig. 3- Simulated PAM 4 modulation at 53.125 GBaud eye diagram out of VCSEL (a) and after MMF fiber propagation and equalization (b).

REFERENCES

[1] D. Gazula, et al. US Patent 20190341743A1, 2020.

[2] C. Rimoldi, et al., Proc. SPIE 12904, 129040L (2024).